Available online at www.sciencedirect.com
SCIENCE DIRECT®
International Journal of Heat and Mass Transfer 47 (2004) 3131–3144
International Journal of HEAT and MASS TRANSFER
www.elsevier.com/locate/ijhmt

Steady natural convection in a vertical cylindrical envelope with adiabatic lateral wall

Y.L. He *, W.Q. Tao, Z.G. Qu, Z.Q. Chen

State Key Lab of Multiphase Flow in Power Engineering, School of Energy and Power Engineering, Xi'an Jiaotong University, Xi'an 710049, China

Received 5 June 2003; received in revised form 13 February 2004

Abstract

The natural convection heat transfer and fluid flow in a vertical cylindrical envelope with constant but different temperatures of the two end surfaces and an adiabatic lateral wall was numerically investigated. Apart from some other applications, it serves as a simplified model of the pulse tube of a pulse tube refrigerator. The simulation was conducted for two end wall temperature differences: $\Delta T_w = 10$ and 220 K. For the cases of $\Delta T_w = 10$ K, it is found that the variation patterns of Nu_L vs. Ra_L within the range of $L/D = 3$–10 are in good consistency with the experimental and theoretical results provided by Catton and Edward for $L/D = 0$–2.5. The C–E chart is thus extended from $L/D = 2.5$ to 10. Within the range of $Ra_L = 1.1 \times 10^5$ to 4×10^7 the fluid isothermals in both longitudinal and cross-sections exhibit some laminated character, and the convective heat transfer rate is in the same order or one-order larger than that of pure heat conduction. For the case of large temperature difference ($\Delta T_w = 220$ K) the natural convection in the enclosure is quite strong in that the convective heat transfer rate is about two-orders larger than that of pure heat conduction which occurs when the cold end is placed down. To reduce the loss of cooling capacity of the pulse tube refrigerator, the pulse tube should be positioned with cold end down. Numerical simulation also revealed that the ratio of the axial length, L, to the diameter, D, has effect on the average heat transfer rate of the envelope under the same other conditions. Within the range of $L/D = 1$–9, the increase in L/D leads to the decrease in heat transfer rate.

Keywords: Natural convection; Vertical cylindrical envelope; Pulse tube refrigerator

1. Introduction

Natural convection in enclosures is a kind of classical problems in heat transfer and numerical heat transfer, and many experimental and theoretical studies have been performed, to name a few, Refs. [1–7] are examples. However, most of the previous investigations were conducted for rectangular enclosures or annulus, a few investigations were conducted for a long cylindrical envelope with an adiabatic lateral wall. Yet such configuration does exist in engineering applications. One typical example is the pulse tube of pulse tube refrigerator. Pulse tube refrigerator is an attracting cryocooler of small capacity widely used in aerospace engineering and for military purpose. The pulse tube itself is a long tube with an inner diameter ranging from several millimeters to tens millimeters. And the ratio of its length to diameter is usually around 10. Its two ends can be regarded as two isothermal surfaces, with its hot end kept at room temperature and the cold end being as low as 80 K, respectively. The pulse tube usually was made of materials with low thermal conductivity and as a first approximation the lateral wall of the tube may be regarded as adiabatic. It may be connected with the pressure wave generator by a long flexible tube with a length of 10 m. Such flexible connectivity between compressor and the cold end allows one to change the

* Corresponding author. Tel.: +86-29-826-63851; fax: +86-29-826-69106.
E-mail address: yalinghe@mail.xjtu.edu.cn (Y.L. He).

0017-9310/$ - see front matter © 2004 Elsevier Ltd. All rights reserved.
doi:10.1016/j.ijheatmasstransfer.2004.02.016

Nomenclature

a	fluid thermal diffusivity
c_p	specific heat at constant pressure
D	diameter
g	gravitational acceleration
GM	cross-sectional axial flow rate
h	heat transfer coefficient
L	length of the cylinder
Nu	Nusselt number
p	pressure
Pr	Prandtl number
q	heat flux
Q	heat transfer rate
r	radius
R	cylinder radius
Ra_L	$g\beta(T_h - T_c)L^3/(av)$
S	source term
SMAX	maximum absolute value of mass flow rate residual of control volume
SSUM	summation of mass flow rate residual of all control volume in the computational domain
T	temperature
u, v, w	velocity component in circumferential, radial and axial coordinate
z	axial coordinate

Greek symbols

β	volume expansion coefficient
Γ	nominal diffusion coefficient
ΔT	temperature difference
λ	fluid thermal conductivity
η	fluid dynamic viscosity
v	fluid kinetic viscosity
θ	inclination angle
ρ	fluid density
ϕ	general variable
φ	circumferential angle

Subscripts

c	cold
cond	conduction
conv	convection
f	fluid
h	hot
m	mean
w	wall

orientation of the pulse tube. The fluid flow in the pulse tube system is oscillating, with frequency ranging from 2 to 10 Hz. The different orientation of the pulse tube leads to different relative positions of the hot and cold ends, which may cause to natural convection in the enclosure when the frequency is low. A pulse tube may be modeled by a cylindrical envelope described in Fig. 1, where the origin of the z coordinate is fixed at the hot end and θ is the angle between the axis of the pulse tube and the gravity. When $\theta = 0$, the hot end is up and the cold end is down; while for $\theta = 180°$, the situation is the opposite. Since for the case with hot end up, the heat transfer in the cylinder is inherently a conduction dominated process, in this paper, only the position with the hot end down is investigated. As a first approximation, in the low frequency region (say several hertz), the natural convection and the forced convection flow are assumed to be additive. Hence, the natural convection in such pulse tube may be studied separately from oscillating flow.

A search of literature only revealed a limited number of related work. Catton and Edwards [1,2] did theoretical and experimental investigations for the natural convection in vertical cylinders heated from below, and provided a general chart, showing the variation patterns of Nusselt number with Ra_L and L/D (hereafter it will be called Catton–Edwards chart, or C–E chart, for simplicity). Their study was limited within $L/D \leqslant 2.5$ and low temperature difference between hot and cold walls. In the work of Thummes et al. [8] investigation was

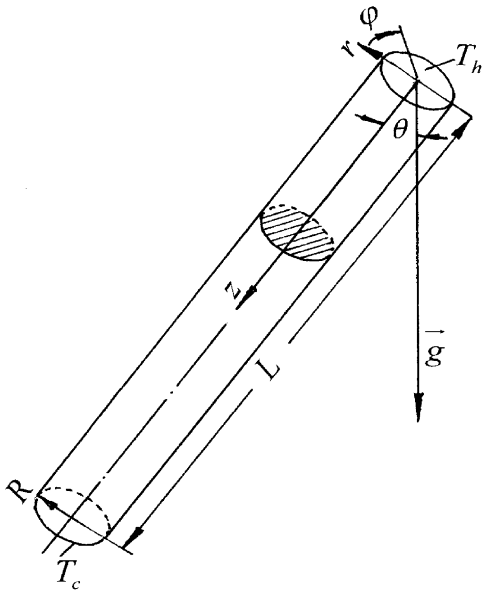

Fig. 1. Three dimensional cylindrical coordinates and the envelope studied.

conducted for a real PTR and a profound effect of the natural convection in the pulse tube on the cooling capacity of a PTR was reported. In [6,7] detailed numerical simulations for the natural convection in a tilted long cylindrical envelope with adiabatic lateral surface were performed, and many peculiar characteristics of convergence process, fluid flow and heat transfer were revealed. However, the studies reported in [6,7] were focused on $L/D = 9$ and $\theta < 180°$.

The purposes of the present study is to perform three dimensional numerical simulation for the natural convection in vertical cylindrical envelopes with adiabatic lateral surface, two isothermal end walls and variable L/D from 1 to 10. The flow in the envelope is assumed to be developed by gravitational force only because of the difference in the fluid density. We do not adopt the Boussinesq assumption, rather, the variation of the thermal properties with temperature are fully taken into account. We take a basic simulation prototype from a pulse tube cryocooler investigated in [9]. For comparison purpose and for extending the C–E chart, computations will be performed for cases with two levels of hot-cold temperature difference, 220 and 10 K, and with L/D varied from 1.0 to 9 for 220 K case and 1–10 for 10 K case.

In the following, the governing equations of the physical problem will be presented first, followed by the numerical methods and some special features of this study. Then numerical results will be provided in detail for the two temperature difference levels. Finally some conclusions will be made.

2. Governing equations and numerical methods

The three dimensional equations for steady-state fluid flow and heat transfer in a cylindrical envelope with variable thermal properties take following form:

$$\frac{\partial}{\partial z}(\rho w\phi)+\frac{1}{r}\frac{\partial}{\partial r}(r\rho v\phi)+\frac{1}{r}\frac{\partial}{\partial \varphi}(\rho u\phi) = \frac{\partial}{\partial z}\left(\Gamma\frac{\partial \phi}{\partial z}\right)+\frac{1}{r}\frac{\partial}{\partial r}\left(\Gamma r\frac{\partial \phi}{\partial r}\right)+\frac{1}{r}\frac{\partial}{\partial \varphi}\left(\frac{\Gamma}{r}\frac{\partial \phi}{\partial \varphi}\right)+S \tag{1}$$

where ϕ is the general variable, representing u, v, w and T, Γ is the general diffusion coefficient, and S is the general source term. For u, v, w, $\Gamma = \eta$, while for T, $\Gamma = \eta/Pr$. For a case with variable thermophysical properties, the general source term for different variables takes following form:

$$w: S = -\frac{\partial p}{\partial z}+\frac{\partial}{\partial z}\left(\eta\frac{\partial w}{\partial z}\right)+\frac{1}{r}\frac{\partial}{\partial r}\left(r\eta\frac{\partial v}{\partial z}\right)+\frac{1}{r}\frac{\partial}{\partial \varphi}\left(\eta\frac{\partial u}{\partial z}\right)+\rho g\cos\theta \tag{2a}$$

$$v: S = -\frac{\partial p}{\partial r}+\frac{\partial}{\partial z}\left(\eta\frac{\partial w}{\partial r}\right)+\frac{1}{r}\frac{\partial}{\partial r}\left(r\eta\frac{\partial v}{\partial r}\right)+\frac{1}{r}\frac{\partial}{\partial \varphi}\left[\eta\frac{r\partial(u/r)}{\partial r}\right]-\frac{2\eta}{r}\left(\frac{1}{r}\frac{\partial u}{\partial \varphi}+\frac{v}{r}\right)+\frac{\rho u^2}{r}-\rho g\sin\theta\cos\varphi \tag{2b}$$

$$u: S = -\frac{1}{r}\frac{\partial p}{\partial \varphi}+\frac{\partial}{\partial z}\left(\eta\frac{\partial w}{r\partial \varphi}\right)+\frac{1}{r}\frac{\partial}{\partial r}\left[r\eta\left(\frac{1}{r}\frac{\partial v}{\partial \varphi}-\frac{u}{r}\right)\right]+\frac{1}{r}\frac{\partial}{\partial \varphi}\left[\eta\left(\frac{1}{r}\frac{\partial u}{\partial \varphi}+\frac{2v}{r}\right)\right]+\frac{\eta}{r}\left[r\frac{\partial(u/r)}{\partial \varphi}+\frac{1}{r}\frac{\partial v}{\partial \varphi}\right]-\frac{\rho vu}{r}+\rho g\sin\theta\sin\varphi \tag{2c}$$

Assuming that $\frac{\partial \eta}{\partial z}, \frac{\partial \eta}{\partial r}, \frac{\partial \eta}{\partial \varphi}$ are small and using the mass conservation law expressed by

$$\frac{\partial w}{\partial z}+\frac{1}{r}\frac{\partial}{\partial r}(rv)+\frac{1}{r}\frac{\partial u}{\partial \varphi}=0 \tag{3}$$

we can obtain following simplified forms for the source terms:

$$w: S = -\frac{\partial p}{\partial z}+\rho g\cos\theta \tag{4a}$$

$$v: S = -\frac{\partial p}{\partial r}+\frac{\rho u^2}{r}-\frac{2\eta}{r^2}\frac{\partial u}{\partial \varphi}-\frac{\eta v}{r^2}-\rho g\sin\theta\cos\varphi \tag{4b}$$

$$u: S = -\frac{1}{r}\frac{\partial p}{\partial \varphi}-\frac{\rho uv}{r}+\frac{2\eta}{r^2}\frac{\partial v}{\partial \varphi}-\frac{\eta u}{r^2}+\rho g\sin\theta\sin\varphi \tag{4c}$$

As can be seen from Fig. 1, the fluid flow and heat transfer are symmetric about the vertical plane through the cylinder axis. Therefore only half of the cylindrical space is taken as the computational domain with the vertical plan through the cylinder axis (where $\varphi = 0$ or π) as a symmetric boundary.

The boundary conditions are as follows:

For u, v, w, at all solid walls, $u = v = w = 0$; at $\varphi = 0$ or π, $u = 0$; $\frac{\partial w}{\partial \varphi} = \frac{\partial v}{\partial \varphi} = 0$.

For T, $T = T_h$ at $z = 0$; $T = T_c$ at $z = L$; at $r = R$, $\frac{\partial T}{\partial r} = 0$. At $\varphi = 0$ or π,

$$\frac{\partial T}{\partial \varphi} = 0 \tag{5}$$

3. Numerical methods

The governing equations are discretized by the finite volume method with practice B in a staggered grid system [10,11]. The diffusion and convection terms are discretized by the power-law scheme. The segregated solution algorithm, SIMPLE, is adopted. The energy

equation is solved simultaneously with the momentum equations. The resulting algebraic equations are solved by the successive line under relaxation method [11]. The boundary conditions are treated by the additional source term method [11] in which the heat flux (including the zero heat flux) at the wall is treated as an additional source of the control volume neighboring with the boundary. The grids are distributed uniformly in the radius and circumferential directions, while in the axial direction, non-uniform distribution is adopted with more grids clustering near the two end walls [6].

The temperature gradient at the hot and cold walls are determined by three-point second-order accurate discretized equation. The grid-independent examination was conducted for the case of the largest temperature difference (220 K) and $L/D = 9$. Nine grid systems were used. They are $13(r)\times13(\varphi)\times48(z)$ (8112 in total), $15\times15\times60$ (13,500 in total), $18\times18\times64$ (20,736), $19\times19\times74$ (26,714), $20\times20\times80$ (32,000), $20\times20\times90$ (36,000), $22\times22\times90$ (43,560), $22\times22\times100$ (48,400), $22\times22\times110$ (53,200), and finally $30\times30\times150$. It is found that starting from the grid system of $20\times20\times80$ the variation of the average heat transfer rate with grid number becomes trivial, with about 3.3% change from $20\times20\times80$ to $30\times30\times150$. The computational time for the later case is more than ten times of that of $20\times20\times80$ grid system. Thus considering both the accuracy and economics, the grid system with $20\times20\times80$ grid points is adopted for the cases of $L/D = 9$ and $\Delta T = 220$ K. In our serial computations for $L/D = 1$–10, the grid number in the radius and circumferential directions were always kept at 20×20, while the grid number in z-direction varied from 30 to 100.

For the case of large temperature difference (~220 K), the problem is a highly non-linear one in that the thermophysical properties varies significantly along the axial direction. From [12] it can be found that within the envelope the thermal physical properties varies from 2.35 (thermal conductivity) to 3.75 times (density). This makes the convergence of the iterative procedure very difficult. After quite a few preliminary computations, it is found that the cross-sectional axial flow rate, symbolized as GM, is an important index to judge the convergence for cases of both large and small end temperature difference

$$GM = \frac{1}{N}\sum_{k=1}^{N}\int_{\Omega_k}\rho(i,j,k)abs(w(i,j,k))r\,\mathrm{d}r\,\mathrm{d}\varphi \qquad (6)$$

Obviously, GM is the section-average axial flow rate.

Two corresponding figures for the cases of $L/D = 9$, $\Delta T = 220$ K and $L/D = 8$, $\Delta T = 10$ K are presented in Fig. 2. From figure it can be seen that for the small ΔT case the value of GM approaches constant after about 1500 iterations, while for the case of large temperature difference, after 18,000 iterations, GM keeps almost

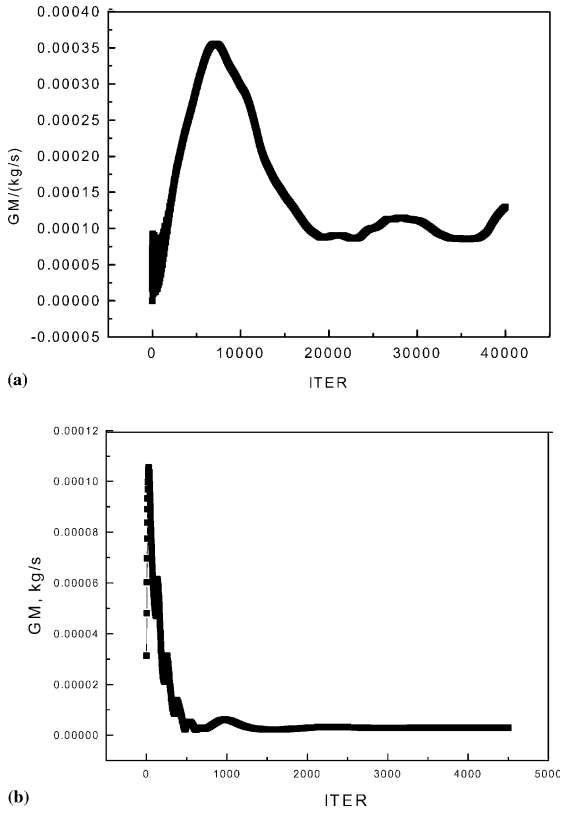

Fig. 2. GM vs. iteration number: (a) $L/D = 9$, $\Delta T = 220$ K, and $Ra_L = 1.596\times10^{10}$; (b) $L/D = 8$, $\Delta T = 10$ K, and $Ra_L = 2\times10^7$.

constant in about consecutive 300 iterations. Beyond that region it changes continuously and never approaches constant again within 40,000 iterations. As discussed in [6] this may be caused by the highly non-linear character of the problem. According to such special feature of iteration process, we select following criteria to judge the convergence of the iterative process for the large temperature difference cases:

(1) the cross-sectional average axial flow rate GM has been beyond the summit of GM–ITER curve and approaches almost constant within 100 iterations;
(2) the relative change in mean heat transfer rate between two consecutive iterations is less than 1.0×10^{-4};
(3) SMAX/GM $\leqslant 1.0\times10^{-6}$;
(4) Abs(SSUM/GM) $\leqslant 1.0\times10^{-7}$,

where SMAX is the absolute maximum value of control volume mass residual, while SSUM is the mass residual of the whole computation domain.

For small temperature difference cases, to compare our numerical results with C–E chart, emphasis was put on the Nusselt number variation with Ra_L, thus condi-

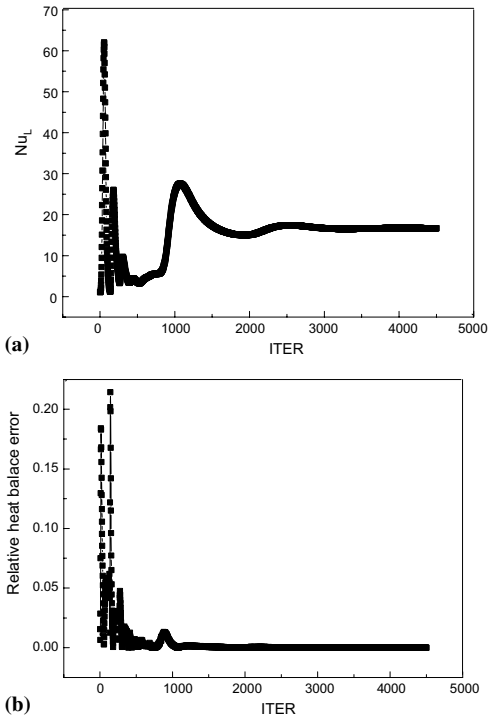

Fig. 3. Convergence process of heat transfer rate: (a) Nu_L vs. ITER, $L/D = 8$, $\Delta T = 10$ K, and $Ra_L = 2 \times 10^7$; (b) relative heat balance with ITER, $L/D = 8$, $\Delta T = 10$ K, and $Ra_L = 2 \times 10^7$.

tion (2) was replaced by that the relative change of Nu_L between consecutive 40 iterations is less than 1.5×10^{-4}, and one more condition is added that the relative difference of heat transfer rates at the two ends is less than 5%. The typical variation process of the two parameters with the iteration number are shown in Fig. 3 for $L/D = 8$.

Numerical simulations were performed for two series of situations, one with $\Delta T = 10$ K ($L/D = 1.0$–10.0), the other with $\Delta T = 220$ K ($L/D = 1.0$–9.0). Although for the first series of situation, the Boussinesq assumption may be used, for the generality of the code developed in our computation the variation of fluid properties with temperature were still taken into account. To make the Rayleigh number, Ra_L, varying in a certain range while kept the ratio of L/D constant, the dimensional value of the tube diameter was changed accordingly. In the second series of computation the PTR described in [9] was taken as its basic mode and the tube diameter was kept constant (27.8 mm). The variation of L/D was implemented via changing the axial length.

In the following, the heat transfer rate (or Nusselt number), temperature and velocity distributions in the enclosures will be presented. The more than 90 numerical cases give too much details of velocity and temperatures distributions to be presented in one paper. We picked up five representative cases for presenting the major results. For simplicity of presentations, the five cases are named A, B, C, D and E as follows:

Case name	A	B	C	D	E
L/D	9	9	3	3	9
ΔT, K	10	10	10	10	220
Ra_L	4×10^7	1.4×10^7	1×10^6	1.4×10^5	1.596×10^{10}

4. Results and discussion

4.1. Results for small temperature difference (case A, B, C and D)

4.1.1. Variation of Nu_L with Ra_L

For small ΔT case computed heat transfer results are presented via the curve of Nu_L vs. Ra_L, where Nu_L and Ra_L take the axial length of the cylinder as the characteristic length. Actually, the value of Nu_L is the ratio of natural convective heat transfer rate to the pure heat conduction through the enclosure. This can be seen easily from following expression:

$$q_{\text{conv}} = h\Delta T = \frac{Nu_L}{L}\lambda_{\text{f}}\Delta T = Nu_L\left(\frac{\lambda_{\text{f}}\Delta T}{L}\right) = Nu_L q_{\text{cond}} \tag{7}$$

The computational results are plotted in the C–E chart (Fig. 4), where below $L/D = 2.5$, our numerical results (smaller black circles) are overlapped with the experimental and analytical results. It can be observed clearly that the Nu_L–Ra_L variation patterns of our numerical data are very consistent with the analytical and experimental results provided by Cartton and Edwards in [1,2]. The major features of this chart can be summarized as follows. (1) With the increase of the value of L/D, the critical Rayleigh number increases below which the heat transfer in the enclosure is dominated by pure heat conduction. (2) For a fixed L/D, with increasing Rayleigh number, the Nusselt number curve climbs up and gradually approaches the curve for zero L/D. In Fig. 4, the solid line was the analytical solution provided by Cartton–Edwards. The white circles are the experimental data of Cartton and Edwards, and all other symbols are our numerical results. The dashed lines are outlined by our numerical results. (3) The larger the value L/D, the steeper the curve of Nu_L–Ra_L, implying the more profound effect of Rayleigh number on Nusselt number. (4) In the range of L/D and Ra_L studied, the ratio of natural convection heat transfer rate within the enclosure over that of the pure heat conduction ranges from 1 to 25 under the same end wall

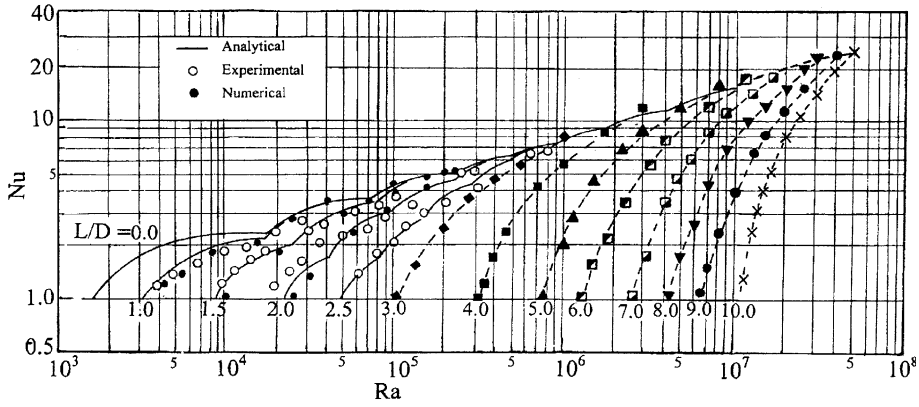

Fig. 4. Extended Cartton–Edwards chart.

temperature difference. For a fixed Ra_L, the smaller the L/D, the larger the ratio.

4.1.2. Temperature distribution

The cross-sectional average fluid temperature distributions along the z-axis are presented in Fig. 5 for $L/D = 3$ and 9. For the convenience of presentation, the vertical plane is put horizontally with the hot end being positioned at the left. This practice will be used later and will not be restated again. It can be seen that with the increase in Rayleigh number, the cross-sectional average fluid temperature becomes more uniform in the major part of the cylinder, and only in the vicinity of the two ends, steep temperature gradient exists. Obviously, when there is no convection in the cylinder, the axial fluid temperature distribution will be a straight line,

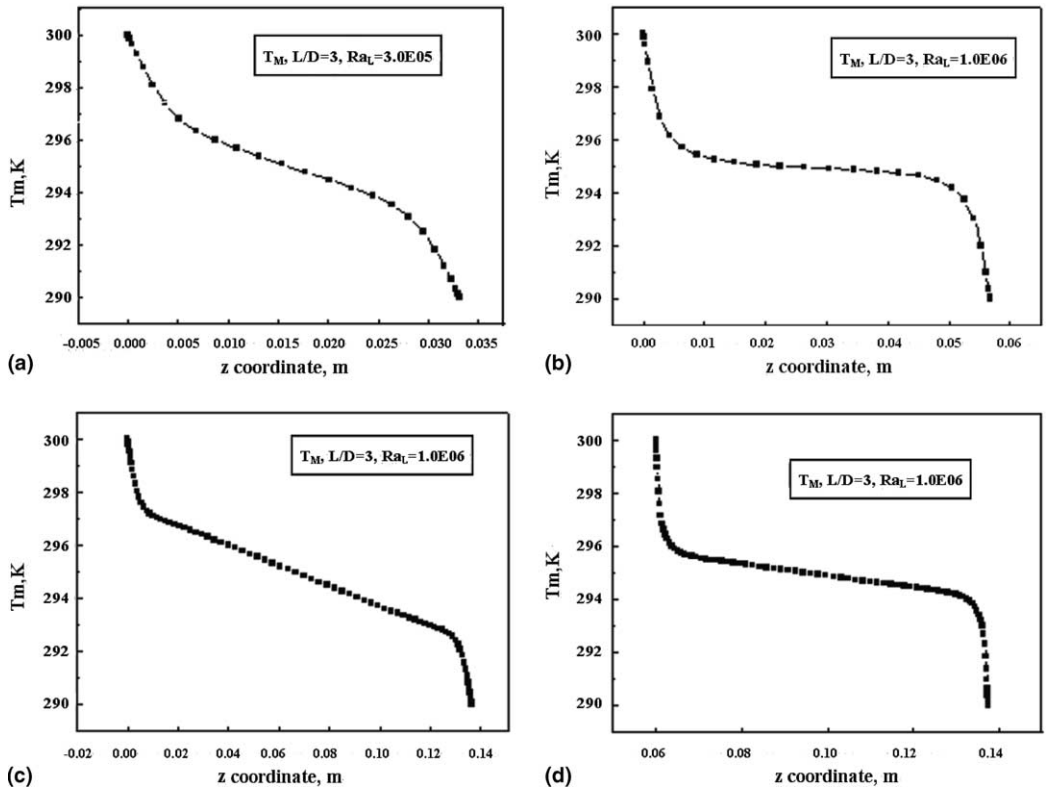

Fig. 5. Sectional average longitudinal fluid temperature distribution: (a) case D; (b) case C; (c) case B; (d) case A.

descending from the hot end to the cold end. The effect of the natural convection is to make the fluid temperature in the center part of the cylinder more or less uniform, and the stronger the convection, the more uniform the temperature distribution in the center part of the cylinder. In Fig. 6, the fluid temperature distribution in the longitudinal section is presented. The effect of the natural convection can be observed more clearly. For small Rayleigh number ($Ra = 1.4 \times 10^5$), the stratified character of the isothermals is quite clear as shown by Fig. 6(a), while for $Ra = 1.0 \times 10^6$, the isothermals become almost vertical to the end wall in the major part of the cylinder, and only in the vicinity of the two ends, the isothermals are parallel to the end wall and become very crowded (Fig. 6(b)). Such variation patterns are consistent with the cross-section average fluid temperature variation curve shown in Fig. 5. For the cases A and B, similar results are obtained and presented in Fig. 6(c) and (d). It can be seen that in the vicinity of the two ends the isothermal are more crowded than that for case C and D (note, in Fig. 6(c) and (d) the two geometric dimensions are not in scale for the clarity of graphic presentation, and the same practice will be adopted in the later presentation of results for $L/D = 9$). The isothermal in the middle transverse section is presented in Fig. 7(a) and (b) for $L/D = 3$. The almost parallel isothermals reflect the characteristics that the fluid streams, flowing from the bottom hot end toward to the top cold end in half of the vertical cylinder and recirculating from top cold end to the bottom hot end in the other half of the cylinder, are more or less laminated in terms of fluid temperature. In the transverse sections near the hot and cold ends, isothermal distributions are shown in Fig. 7(c) and (d) for case B. Apart from the difference in temperature level, the isothermals near the hot end exhibits some special features. As indicated above, a global circulation exits in the entire cylindrical envelope. In half of the cylinder, fluid goes up and in the other half it goes

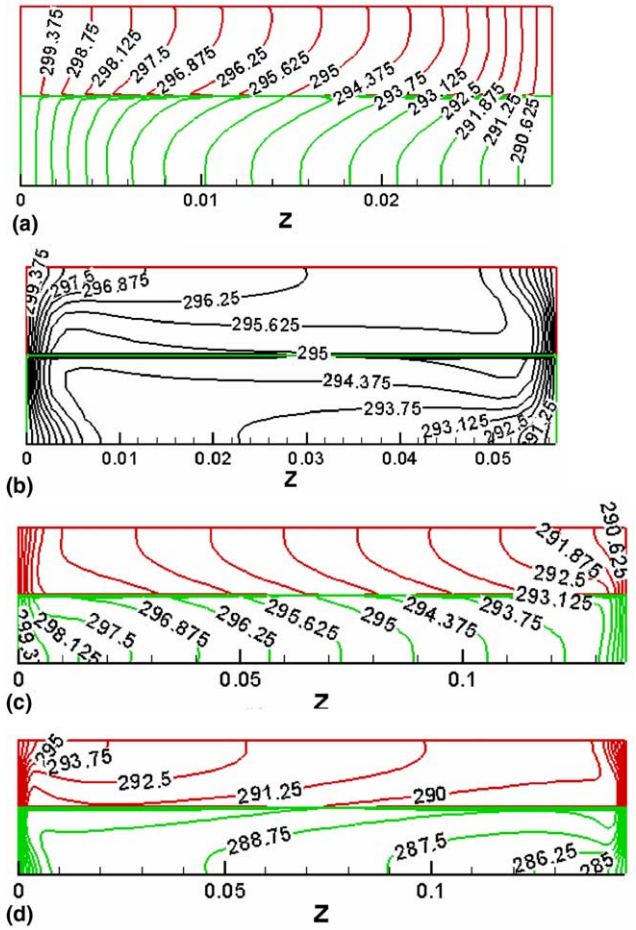

Fig. 6. Fluid temperature distribution in the longitudinal section of the cylinder: (a) $Ra = 1.4 \times 10^5$ (case D); (b) $Ra = 1 \times 10^6$ (case C); (c) $Ra = 1.4 \times 10^7$ (case B); (d) $Ra = 4 \times 10^7$ (case A).

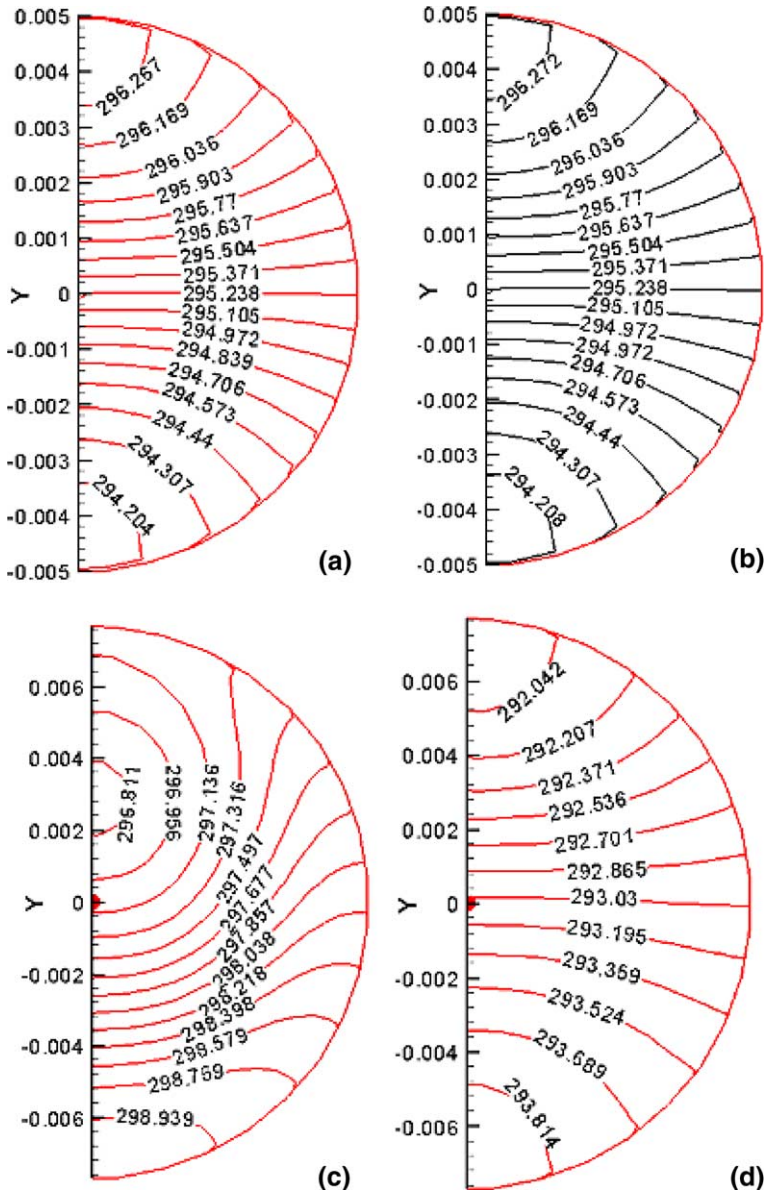

Fig. 7. Cross-sectional fluid isothermals for $L/D = 3$ and 9: (a) middle cross-section, $Ra = 1.4 \times 10^5$ (case D); (b) middle cross-section, $Ra = 1.0 \times 10^6$ (case C); (c) near the hot end ($L/D = 9$); (d) near the cold end ($L/D = 9$).

down. At the same axial cross-section, the fluid temperature in the upward part is obviously higher than that in the downstream part. Such kind of feature can be clearly observed in Fig. 7(c), where the downstream fluid isothermal consists of a series of circles, centered by the one with $T = 296.811$ K, while the temperatures of the upstream fluid are basically at the level of 298 K. Fig. 7(d) exhibits the same feature with less difference between the upstream part and the downstream part. The global circulation will be observed more clearly from the following presentation of velocity fields.

4.1.3. Velocity distribution

Velocity vectors in the longitudinal section for the four cases are presented in Fig. 8, where the global circulation of the stream can be clearly observed. This global circulation is composed of two branches: one with higher temperature and going upward and the other with lower temperature going downward. Apart from this global circulation, some local small recirculations exist. This can be found from the velocity distribution near the hot and cold end. Fig. 9 provides such pictures for the case A, where two small recirculations can be

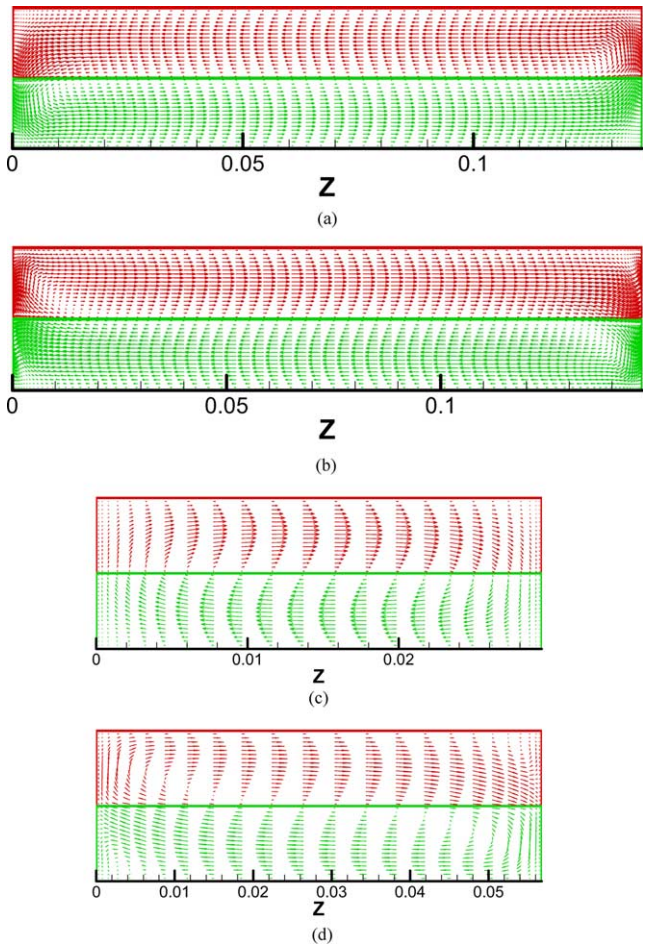

Fig. 8. Longitudinal velocity distribution of cases A, B, C and D: (a) $Ra = 1.4 \times 10^7$ (case B); (b) $Ra = 4 \times 10^7$ (case A); (c) $Ra = 1.4 \times 10^7$ (case D); (d) $Ra = 1.0 \times 10^7$ (case C).

spotted. The longitudinal section is the symmetric surface, where the circumferential component, i.e., u-component, equals zero. At the other locations of any cross-section, u-component exits, making the flow pattern three dimensional. In Fig. 10, the velocity distributions at nine cross-sections of case A are presented for illustration. In order to easily identify the velocity direction, the circumferential grid lines are reserved. It can be seen that the fluid flow at the nine cross-sections does not form a closed circulation. The fluid either goes upward or downward to form a local closed circulation, making the flow pattern quite complicated. Because of such multi-vortex structure of the flow field, the fluid possess circumferential velocity component, even though from the vertical geometry, only axial and radial velocity components can be easily expected. Such seemingly abnormal phenomenon is probably an inherent character of the natural convection in enclosures. For example, Powe et al. [13] found experimentally that for the natural convection in cylindrical annuli, the flow pattern is not symmetric to the vertical axis when the Rayleigh number is within a certain range, even though the geometry and the boundary conditions are symmetric about the vertical axis.

4.2. Results for large temperature difference (case E)

4.2.1. Heat transfer rate and sectional average axial flow rate

The Rayleigh number of case E is about three-order larger than that of case A (Table 1), even though case A and E have the same dimensional axial length. From the definition of Rayleigh number, $Ra = (\rho^2 g \beta \Delta T L^3/\eta^2)Pr$, the large difference in Ra_L comes from the difference in ΔT and thermal physical properties. The natural convection in the enclosure of case E is much stronger than that of case A, as can be witnessed from the difference in the axial flow rate GM, for case A $GM = 4.562 \times 10^{-6}$

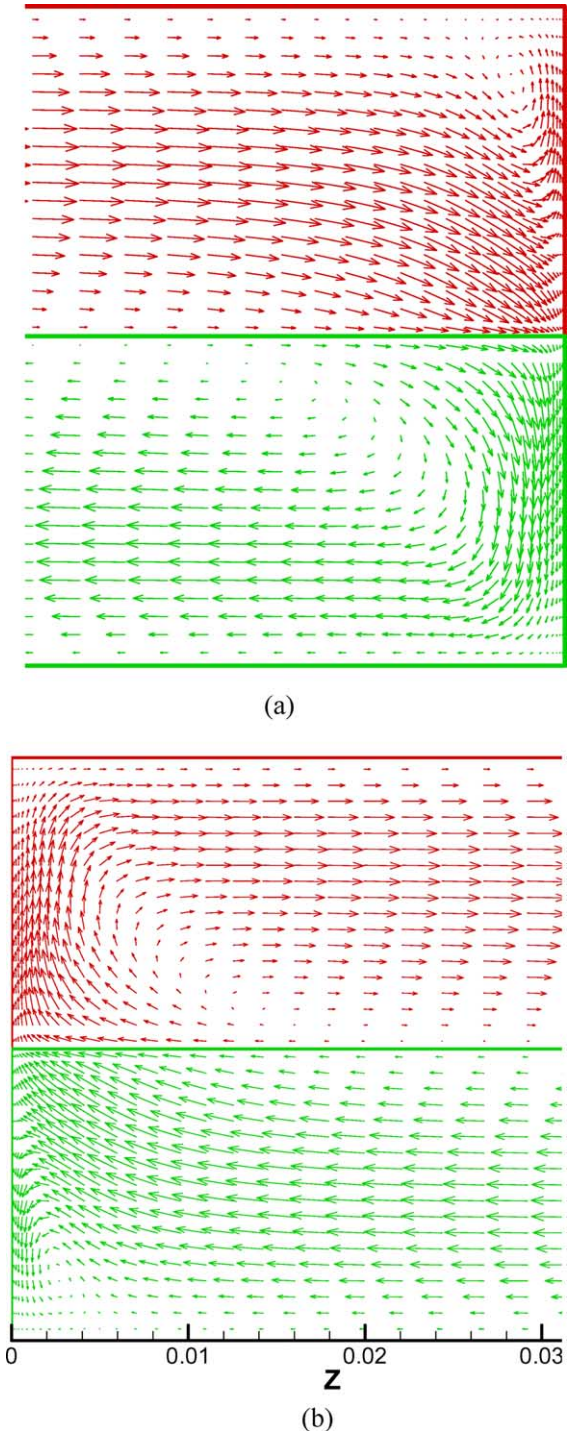

Fig. 9. Detailed longitudinal velocity distribution near two ends of case A: (a) flow pattern near the cold end; (b) flow pattern near the hot end.

kg/s, while for case E GM $= 8.739 \times 10^{-5}$ kg/s. The predicted values of Nu_L, heat transfer rate and pure heat conduction rate of the fives cases are listed in Table 1, where the pure heat conduction was computed from the 1-D heat conduction equation assuming that the transport process was pure diffusive between the hot and cold ends and the mean fluid thermal conductivity was used. The mean thermal conductivity was determined from volume average one of the entire domain.

Velocity and isothermal distributions in the longitudinal and cross-sections for case E reveal that the flow pattern of case E is much more complicated than that of case, A, characterized by a multi-vortex structure in both longitudinal and transverse sections imposed on the global circulation between the hot and cold ends. Such distributions were partially presented in [7], and interested readers may consult that reference. In the following only the effect of L/D on heat transfer rate is presented.

It worth noting that the Rayleigh number based on L for case E is as high as 10^{10}, a question may arise as whether the laminar model is appropriate for this situation. For rectangular enclosure with two opposing vertical walls maintaining at constant but different temperatures, the fluid flow starts from very low Rayleigh number (much less than 1000) and the laminar flow usually restricted below $Ra_L < 10^8$ [4]. For the case studied, however, the driving force of the flow—temperature difference comes from the top and bottom walls and the lateral wall is assumed to be adiabatic. Then from extended C–E chart, it can be seen that the fluid will keep still until the Rayleigh number based on the enclosure height becomes larger than a certain value. For example, for L/D equals 10, this value is as high as 10^7. Thus it is the authors' believe that three-order increase in the Rayleigh number will not make the flow to be turbulent.

4.2.2. The effect of L/D on the heat transfer rate

From heat transfer point of view, it is interesting to reveal the effect of L/D on the heat transfer in the envelope with the same temperature difference between hot and cold ends (220 K) and the same tube diameter. Computations were conducted for other eight situations with L/D varying from 8 to 1. The average heat transfer rate in the envelope for different L/D situations are presented in Fig. 11(a). As seen there, the increase in L/D leads to the decrease in the average heat transfer rate. In the L/D range studied, this decrease is caused by the fact that the increase of the space distance between the hot and cold ends actually leads to a weaker fluid flow under the same driving force of temperature difference.

In Fig. 11(b) and (c), the section average fluid temperatures are presented for $L/D = 1$ and 9, respectively. Two features may be noted. First, near the two ends, the temperature gradients are very large, because heat is transferred just by conduction at the end walls. Second,

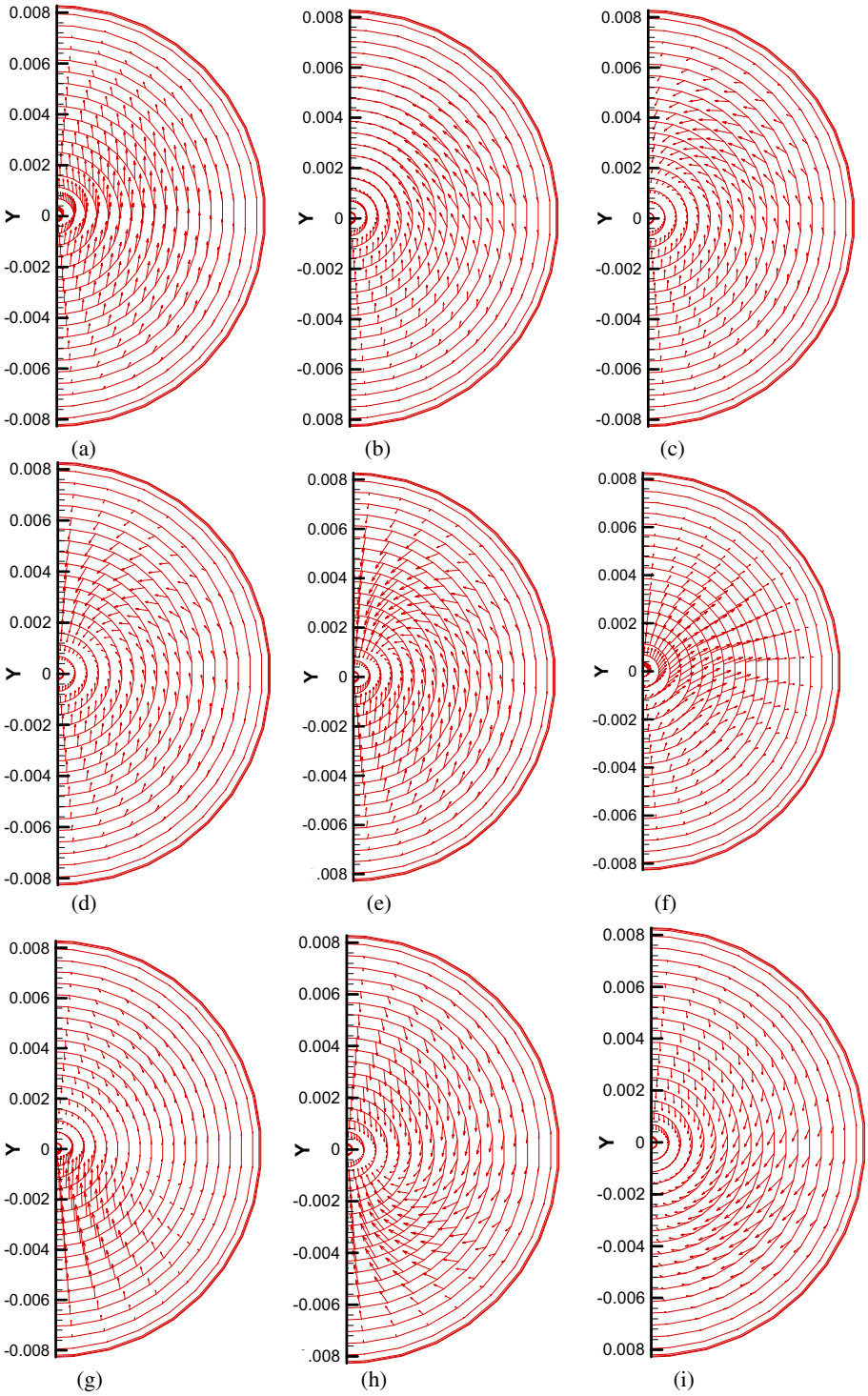

Fig. 10. Velocity distributions at nine cross-sections of case A ($L/D = 9$, $Ra = 4 \times 10^7$): (a) $z = 0.011$ m; (b) $z = 0.032$ m; (c) $z = 0.059$ m; (d) $z = 0.087$ m; (e) $z = 0.119$ m; (f) $z = 0.15$ m; (g) $z = 0.18$ m; (h) $z = 0.21$ m; (i) $z = 0.239$ m.

the temperature gradient near the cold end is appreciably larger than that of hot end, because the large difference in the fluid thermal conductivity near the two ends. It is to be noted that, for the situation of $L/D = 1$,

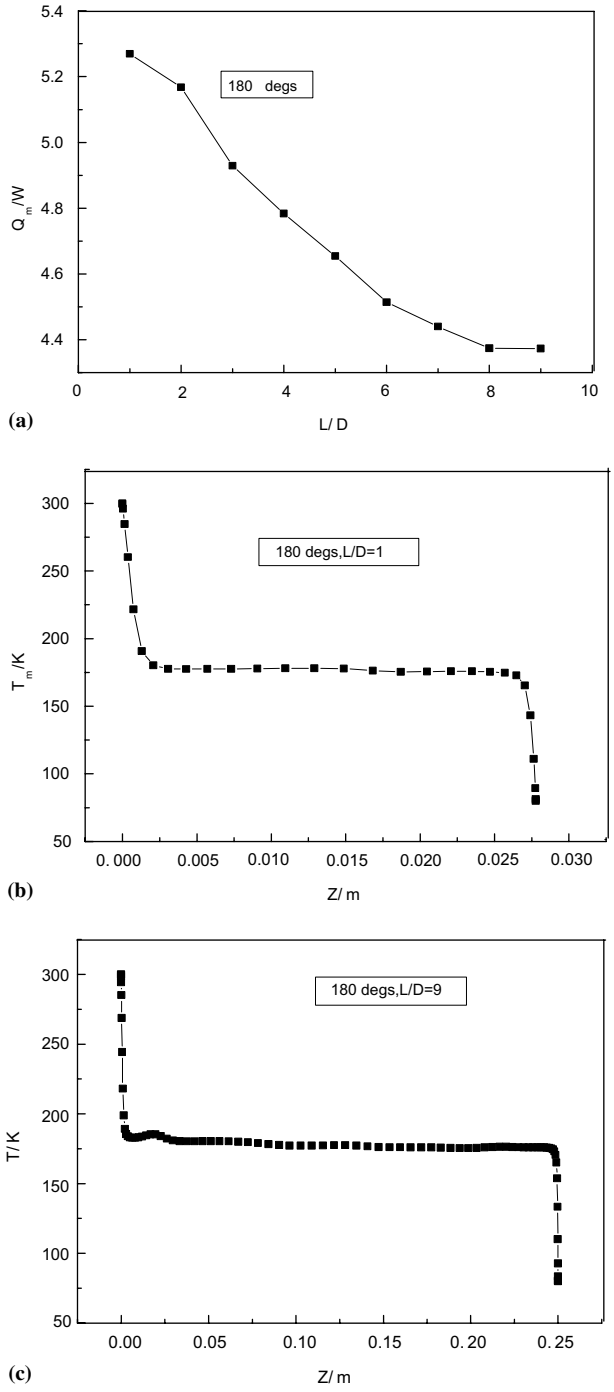

Fig. 11. Heat transfer characteristics for case E at different L/D: (a) variation of average heat transfer rate with L/D; (b) cross-sectional average fluid temperature for $L/D = 1$; (c) cross-sectional average fluid temperature for $L/D = 9$.

the height of the envelope is 1/9 of that for $L/D = 9$, thus the end wall temperature gradient of $L/D = 1$ is actually larger than that of $L/D = 9$, reflecting the larger heat transfer rate of the shorter envelope.

Table 1
Predicted Nusselt number and heat transfer rate

Case	A	B	C	D	E
Ra_L	4×10^7	1.4×10^7	1×10^6	1.4×10^5	1.596×10^{10}
Nu_L	24.06	8.22	8.08	1.597	105.48
Q_{conv}, W	7.572×10^{-3}	9.774×10^{-4}	8.919×10^{-3}	7.185×10^{-3}	4.388
Q_{cond}, W	2.06×10^{-3}	2.734×10^{-4}	3.656×10^{-3}	1.896×10^{-3}	2.838×10^{-2}

5. Conclusions

The natural convection in a vertical cylindrical envelope with top and bottom ends maintained at lower and higher temperatures and the lateral surface adiabatic was simulated by three dimensional model with varying thermophysical properties. Two levels of the end temperature difference, $\Delta T_w = 10$ and 220 K, were simulated. The major findings are as follows.

1. For the small ΔT_w cases (A, B, C and D), numerical results of the Nusselt number for L/D from 3 to 10 are in good consistency with the experimental and theoretical results provided by Catton and Edward. And the C–E chart is extended from $L/D = 2.5$ to 10. The two important features of the C–E chart are (1) the larger the ratio of L/D, the more profound the effect of Ra_L on Nu_L; (2) within the range of L/D studied, with the increase in Rayleigh number the value of Nu_L gradually approaching the theoretical results obtained for $L/D = 0$.
2. For the small ΔT_w cases studied ($Ra_L = 1.1 \times 10^5 \sim 4 \times 10^7$), there is a global circulation between the hot and cold ends, accompanied by some local recirculations in the envelope. Generally speaking, the natural convection is not very strong in that the convective heat transfer rate is about the same order, or one-order larger than that of pure heat conduction, and the flow structure is not very complicated characterized by a global circulation accompanied by some local recirculation in longitudinal section. Hence the fluid temperature isothermals both in longitudinal section and cross-section exhibit some regularly laminated character.
3. For case E, it is found that the heat transfer rate is about two-orders larger than that of the pure heat conduction. Thus for the device like pulse tube refrigerator, the operational position of the pulse tube is recommended to be positioned with cold end down in order to reduce the loss of the cooling capacity.
4. For the large temperature difference case, with the decrease in L/D, the average heat transfer rate increases. This also gives some hints for relative devices in order to reduce the loss of energy to the environment by natural convection in enclosure.

Acknowledgements

This work is supported by the National Key Project of Fundamental R&D of China (grant number 2000026303) and National Natural Science Foundation of China (grant number 50276046).

References

[1] I. Catton, D.K. Edwards, Effect of side walls on natural convection between horizontal plates heated from below, ASME J. Heat Transfer 90 (1967) 295–299.
[2] D.K. Edwards, I. Catton, Prediction of heat transfer by natural convection in closed cylinders heated from below, Int. J. Heat Mass Transfer 12 (1969) 25–30.
[3] T.H. Kuhen, R.J. Goldstein, An experimental and theoretical study of natural convection in the annulus between horizontal concentric cylinders, J. Fluid Mech. 74 (1976) 605–719.
[4] G. Barakos, E. Mitsoulis, Natural convection flow in a square cavity revisited: laminar and turbulent models with wall function, Int. J. Numer. Meth. Fluid 18 (1994) 695–719.
[5] J.G. Wei, W.Q. Tao, Numerical study of natural convection in a vertical annulus with constant heat flux on the inner wall, Int. J. Numer. Meth. Heat Fluid Flow 6 (1996) 31–46.
[6] Y.L. He, W.Q. Tao, T.S. Zhao, Z.Q. Chen, Natural convection in a tilted long cylindrical envelope with lateral adiabatic surface, Part 1: theoretical modeling, numerical treatments, Numer. Heat Transfer, Part A 44 (2003) 375–397.
[7] Y.L. He, W.Q. Tao, T.S. Zhao, Z.Q. Chen, Natural convection in a tilted long cylindrical envelope with lateral adiabatic surface, Part 2, heat transfer rate, flow patterns and temperature distributions, Numer. Heat Transfer, Part A 44 (2003) 399–431.
[8] G. Thummes, M. Schreiber, R. Landgraf, C. Heiden, Convective heat losses in pulse tube coolers: effect of pulse tube inclination, in: R.G. Ross (Ed.), Cryocoolers 9, Plenum Press, New York, 1997.
[9] Y.L. He, Theoretical and experimental investigations on the performance improvements of split-Stirling refrigerator and pulse tube cryocooler. PhD thesis, School of Energy and Power Engineering, Xi'an Jiaotong University, Xi'an, China, 2002.
[10] S.V. Patankar, Numerical Heat Transfer and Fluid Flow, McGraw-Hill, New York, 1980.

[11] W.Q. Tao, Numerical Heat Transfer, second ed., Xi'an Jiaotong University Press, Xi'an, 2001.
[12] R.F. Barron, Cryogenic Heat Transfer, Taylor and Francis, New York, 1999.
[13] R.E. Powe, C.T. Carley, E.H. Bishop, Free convection flow pattern in cylindrical annuli, ASME J. Heat Transfer 91 (1969) 310–314.